Safety of Quark/Gluon Jet Classification

Alexis Romero, Daniel Whiteson, and Michael Fenton
Department of Physics and Astronomy, University of California, Irvine, CA 92627

Julian Collado and Pierre Baldi
Department of Computer Science, University of California, Irvine, CA 92627

(Dated: March 17, 2021)

The classification of jets as quark- versus gluon-initiated is an important yet challenging task in the analysis of data from high-energy particle collisions and in the search for physics beyond the Standard Model. The recent integration of deep neural networks operating on low-level detector information has resulted in significant improvements in the classification power of quark/gluon jet tagging models. However, the improved power of such models trained on simulated samples has come at the cost of reduced interpretability, raising concerns about their reliability. We elucidate the physics behind quark/gluon jet classification decisions by comparing the performance of networks with and without constraints of infrared and collinear safety, and identify the nature of the unsafe information by revealing the energy and angular dependence of the learned models. This in turn allows us to approximate the performance of the low-level networks (by 99% or higher) using equivalent sets of interpretable high-level observables, which can be used to probe the fidelity of the simulated samples and define systematic uncertainties.

I. INTRODUCTION

Data from experiments at the Large Hadron Collider (LHC) probe some of the most fundamental questions in modern science, such as the nature of dark matter, the potential unification of forces, and the matter/anti-matter imbalance in the observable universe. In recent years, the integration of machine learning into data analyses has catalyzed scientific advances in particle physics, as the machine-learned models are able to handle data of greater complexity and higher dimensionality than previously feasible [1–4]. However, the improved power of such models often comes at the cost of reduced interpretability. As most models are trained on simulated samples using supervised learning techniques, physicists are rightly concerned that models may base their classification or regression decisions on portions of the feature space which are poorly described by simulations, or where the modeling is theoretically uncertain. For this reason, it is important that physicists be able to understand the nature of the information being used, providing confidence in the network decisions, and allowing the assessment of systematic uncertainties.

One important application of machine learning is the classification of quark versus gluon jets [5–11]. While significant efforts have been made to improve classification performance, less attention [12] has been paid to understanding the Quantum Chromodynamics (QCD) nature of the information being used. Two main classes of QCD effects can be considered: perturbative and non-perturbative. Although there is no universal and gauge-invariant way to distinguish between the two, physicists have relied on principles such as infrared and collinear (IRC) safety to identify perturbative effects, as IRC-safety ensures that observables are invariant to soft emissions and arbitrary collinear parton splittings. Studies in simulated quark/gluon dijet samples indicate that the task of quark/gluon tagging should be dependent only on IRC-safe observables, as the likelihood for quark vs. gluon classification is IRC-safe [13]. Nevertheless, networks trained on high-level information of quark/gluon jet samples simulated with hadronization effects often outperform those trained on high-level information of samples simulated before hadronization ("at parton level"), indicating that quark/gluon tagging is highly sensitive to both perturbative and non-perturbative effects [9, 13]. Given that the current theoretical understanding of non-perturbative effects like hadronization is limited, as well as a lack of a current unambiguous definition of quark and gluon jets at the hadron level, variations in the modeling of non-perturbative effects with different parton-shower event generators can occur, thus hindering our abilities to calculate the systematic uncertainties of the low-level models.

Here we focus directly on the question of the nature of the QCD information used by networks that learn to classify quark and gluon jets from low-level calorimeter information. Our strategy is to identify the source and importance of the perturbative and non-perturbative effects by comparing the performance of networks whose internal structures enforce IRC-safety to those which are unconstrained, on benchmark problems with and without hadronization effects, and as a function of jet energy. A drop in performance for the networks that enforce IRC-safety relative to the unconstrained networks is attributed to IRC-unsafe information. We then attempt to more specifically identify the nature of the IRC-unsafe information by employing networks whose internal structure enforces prescribed IRC-unsafe dependencies on transverse momentum and angular distance metrics. This strategy allows us to reveal the nature of the IRC-unsafe information by narrowing down its energy and angular dependence, enabling us to map it to well-known IRC-unsafe jet variables, such as tower multiplic-

ity, IRC-unsafe generalized angularities [14], and energy-flow polynomials (EFPs) [15]. Capturing the information used by low-level networks into high-level observables is vital for future applications of machine learning classifiers [16], as it enables physicists to both understand the nature of the information and improve confidence in the network's decisions by allowing for intentional inclusion or exclusion of such information.

The rest of this paper is organized as follows. Section II lays out the strategy used to reveal the reliance of the low-level networks on IRC-safe and IRC-unsafe information, and for capturing this information into high-level observables. Section III describes the data generation settings. Results and discussion are presented in Section IV, and conclusions in Section V.

II. STRATEGY AND METHODS

Two key elements for understanding the nature of the information used by machine learning classifiers for jet tagging are the inherent constraints of the classifier and the jet representation.

In recent studies, many jet representations have been considered; popular choices include: jet images [1, 17, 18], unordered sets of constituents [19, 20], and ordered sets of constituents [2, 21–23]. In order to compare each of the learning strategies on equal footing and to maintain the maximal amount of information, we choose to represent the jets as unordered sets of calorimeter towers. The towers in the sets are characterized by their three-momenta – $(p_{\mathrm{T}}, \eta, \phi)$ – and are centered with respect to the $E-$scheme jet axis. Only towers within a radial distance of $R = \sqrt{\Delta\phi^2 + \Delta\eta^2} < 0.4$ from the jet axis are kept.

The first step in our strategy focuses on assessing the importance of IRC-safe information calculated from the unordered sets of calorimeter towers. First, we estimate an effective upper limit on the performance of quark/gluon classifiers by employing Particle-Flow Networks (PFNs) [19]. PFNs have consistently achieved top performances for quark/gluon jet classification [10, 19, 20, 24], so their performance is taken to be the benchmark to which all other networks in this paper are compared. Next, we consider Energy-Flow Networks (EFNs) [19] which, like PFNs, treat jets as unordered sets of constituents, but use an architecture which constrains internal functions to forms which enforce IRC-safety. We assess the importance of IRC-safe information by comparing the difference in performance between the PFNs and the EFNs. A reduced performance by the EFNs relative to the PFNs would suggest that the PFNs are relying on IRC-unsafe information.

The second step focuses on exploring the nature of the IRC-unsafe information. We begin by introducing EFN[κ]s, a generalization of EFNs whose architecture constrains the models to use internal functions with a given energy weighting exponent, κ. Variation of the network performance with κ reveals the nature of the functional forms which capture the IRC-unsafe information. We then attempt to map this information onto families of IRC-unsafe observables, which can be concatenated to IRC-safe observables to match the performance of the PFNs. Two families of IRC-safe observables are used: N-subjettiness variables in combination with jet mass, and IRC-safe EFPs. Similarly, two families of IRC-unsafe observables are used: IRC-unsafe generalized angularities and IRC-unsafe EFPs, both in combination with tower multiplicity.

The networks employed in our analysis of the information used during quark/gluon jet classification are detailed below.

A. Particle-Flow Networks

The power of PFNs relies on their ability to learn virtually any symmetric function of the towers. Their mathematical structure is naturally invariant under permutation of the input ordering, as it is built on a summation over the towers. PFNs can be mathematically summarized as

$$\mathrm{PFN}: F\left(\sum_{i\in\mathrm{jet}} \Phi(p_{\mathrm{T}i}, \eta_i, \phi_i)\right), \qquad (1)$$

where Φ represents the per-tower latent space and F the event-level latent space. The transverse momentum, pseudorapidity, and azimuthal angle of tower i are respectively given by $p_{\mathrm{T}i}$, η_i, and ϕ_i, and this notation is used throughout this paper when indexing over the towers in a jet.

We place no constraints on the nature of the latent spaces, giving the network great flexibility. For this reason, they are a useful probe of the effective upper limit of the performance in the classification tasks when minimal constraints are applied to the nature of the learning method[1].

B. Energy-Flow Networks

Similar in structure to PFNs, EFNs are constructed such that the event-level latent space learns functions which have a linear energy factor. Mathematically, EFNs can be summarized as

$$\mathrm{EFN}: F\left(\sum_{i\in\mathrm{jet}} p_{\mathrm{T}i}\Phi(\eta_i, \phi_i)\right), \qquad (2)$$

[1] We verified in several cases that similar performance is achieved by convolutional neural networks operating on jet images, but due to the significantly increased computational cost and number of parameters, we set them aside as probes of the upper bound in favor of PFNs.

where unlike in PFNs, $\Phi(\eta_i, \phi_i)$ is a function only of the angles, weighted by a linear term in transverse momentum, $p_{\mathrm{T}i}$, as required for IRC-safety.

C. IRC-unsafe Energy-Flow Networks

In anticipation of the importance of IRC-unsafe information, we introduce a generalization of EFNs which includes non-linear energy weighting exponents. Mathematically, Eq. 2 is modified to be non-linear in $p_{\mathrm{T}i}$ as

$$\mathrm{EFN}[\kappa] : F\left(\sum_{i\in\mathrm{jet}} p^{\kappa}_{\mathrm{T}i}\Phi(\eta_i, \phi_i)\right), \tag{3}$$

where $\mathrm{EFN}[\kappa]$ refers to the modified form of an EFN with an energy factor of degree κ, which is referred to as the *energy weighting exponent* in this paper[2]. This modification allows us isolate the critical values of $\kappa \neq 1$ that capture most of the IRC-unsafe information needed for the quark/gluon classification task. Note that $\mathrm{EFN}[\kappa]$ can also be used to explore IR-safe energy weighting factors by setting $\kappa > 1$.

D. High-level Observables

The literature on strategies for quark/gluon classification using high-level observables is quite mature, providing many families of high-level observables which reduce the large dimensionality of the input space into one-dimensional observables that retain useful information for classification. These observables have the significant advantages that they are physically interpretable, compact, and allow for reasonable assessment of systematic uncertainties due to, for example, mismodeling in simulation. The disadvantage is that they are limited to those ideas conceived of by human physicists. In our study, the observables are calculated directly from the calorimeter towers, and are paired with fully connected Dense Neural Networks (DNNs) or with Linear Discriminant Analysis (LDA) classification models in the cases where the observables are linearly separable, such as EFPs.

We consider the following IRC-safe observables that are traditionally used in quark/gluon studies:

- N-subjettiness variables [25, 26], which provide a measure of the degree to which the radiation within a jet is aligned along N candidate subjet axes, and are defined as

$$\tau_N[\beta] = \sum_{i\in\mathrm{jet}} p_{\mathrm{T}i}\min\{R^{\beta}_{i,1}, R^{\beta}_{i,2}, \ldots, R^{\beta}_{i,N}\}, \tag{4}$$

  where $R_{i,J}$ is the angular distance between subjet axis J ($J \leq N$) and tower i. The parameter β ($\beta > 0$) is referred to as the *angular weighting exponent* in this paper. Following [27], we compute the first 18 N-subjettiness observables with respect to the k_{T} axis:

$$\{\tau_1[\beta = \tfrac{1}{2}], \tau_1[\beta = 1], \tau_1[\beta = 2], \ldots,$$
$$\tau_6[\beta = \tfrac{1}{2}], \tau_6[\beta = 1], \tau_6[\beta = 2]\}.$$

- Jet mass (m_{jet}), which has been found to be a powerful quark/gluon jet discriminant [6].

- IRC-safe Energy-Flow Polynomials [15], which are sets of non-isomorphic multigraphs that linearly span the space of IRC-safe observables. For a multigraph G with V vertices and edges $(k, l) \in G$, the corresponding EFP observable is defined as

$$\mathrm{EFP}[\beta] = \sum_{i_1\in\mathrm{jet}} \cdots \sum_{i_V\in\mathrm{jet}} p_{\mathrm{T}i_1} \cdots p_{\mathrm{T}i_V} \prod_{(k,l)\in G} R^{\beta}_{i_k,i_l} \tag{5}$$

  where R_{ij} is the angular distance between particles i and j. Following [15], the optimal performance for quark/gluon jet classification using IRC-safe EFPs is achieved with $\beta = \frac{1}{2}$; we employ the same set for our studies, with a maximum number of edges of $d \leq 5$, where d corresponds to the degree of the angular monomial.

Distributions of a selection of N-subjettiness and IRC-safe EFP observables are shown in Fig. 1.

To capture the IRC-unsafe information, we consider the following IRC-unsafe observables:

- IRC-unsafe Generalized Angularities [14], which have a simple form that allows for easy interpretation, are defined as

$$\lambda[\kappa, \beta] = \sum_{i\in\mathrm{jet}} p^{\kappa}_{\mathrm{T}i}\left(\frac{R_{i,\mathrm{jet}}}{R}\right)^{\beta}, \tag{6}$$

  where $R_{i,\mathrm{jet}}$ is the radial distance from tower i to the k_T jet axis, and R is the jet radius.

- IRC-unsafe Energy-Flow Polynomials [15], which have a similar form to the IRC-safe EFPs in Eq. 5, but with a non-linear energy weighting exponent ($\kappa \neq 1$). Following the notation in Eq. 5, the IRC-unsafe EFPs are defined as

$$\mathrm{EFP}[\kappa, \beta] = \sum_{i_1\in\mathrm{jet}} \cdots \sum_{i_N\in\mathrm{jet}} p^{\kappa}_{\mathrm{T}i_1} \cdots p^{\kappa}_{\mathrm{T}i_N} \prod_{(k,l)\in G} R^{\beta}_{i_k i_l}. \tag{7}$$

---

[2] Two equivalent approaches can be used to implement $\mathrm{EFN}[\kappa]$: (1) elevating the tower's transverse momentum from p_{T} to p^{κ}_{T}, and then then passing them as input to the EFN, and (2) directly modifying the architecture of the EFN to use p^{κ}_{T} as the weighting parameter of $\Phi(\eta_i, \phi_i)$ in Eq. 2.

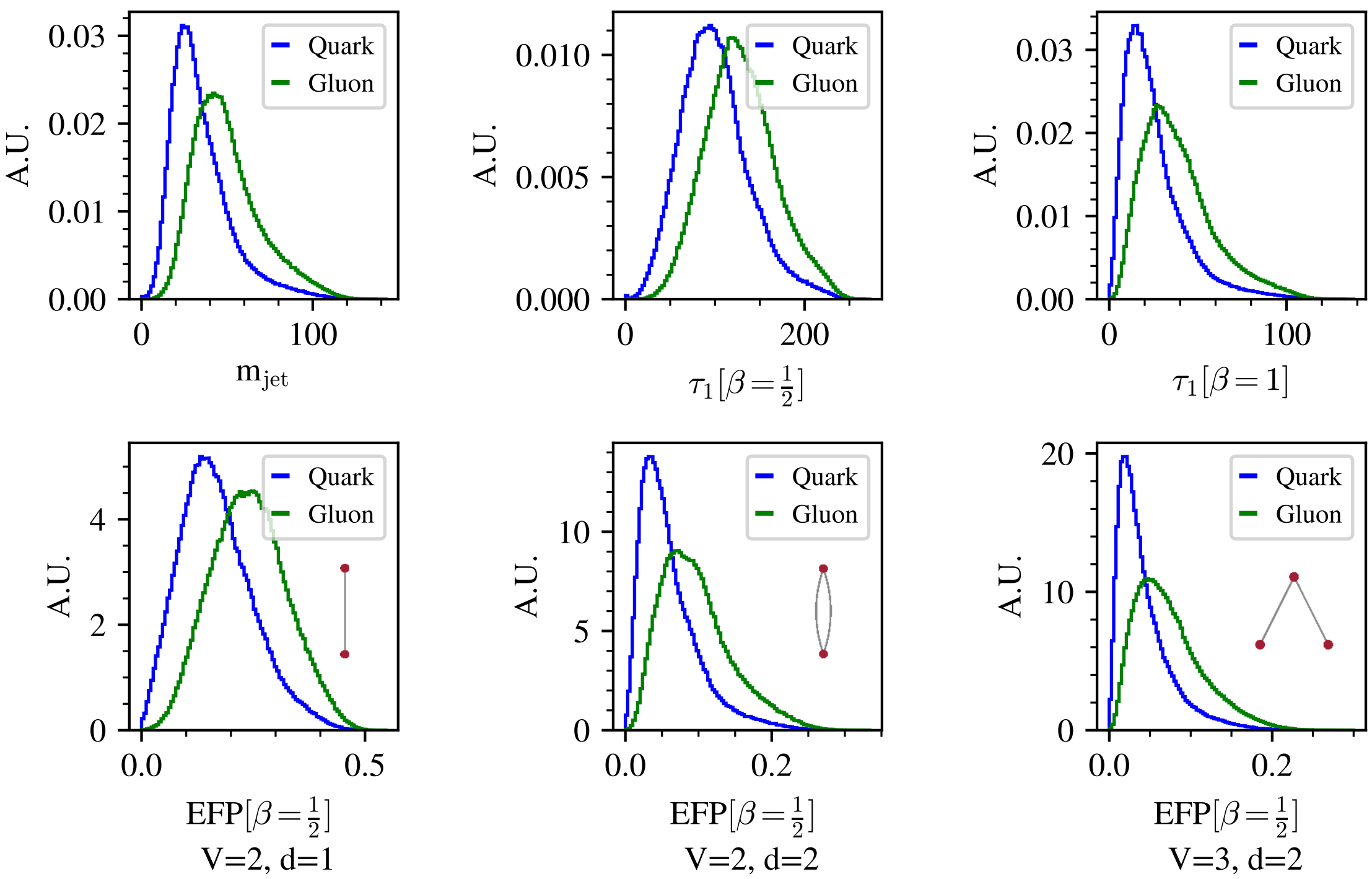

FIG. 1. Distributions of jet mass and select N-subjettiness observables (top), and IRC-safe EFP observables (bottom), for quark- and gluon-initiated jets with $p_T \in [500, 550]$ GeV. The shape of the EFP multigraphs is shown for illustrative purposes.

- Tower multiplicity (n_t), which counts the number of towers in a jet and has also been found to be a powerful quark/gluon jet discriminant [6].

Distributions of a selection of IRC-unsafe generalized angularity and IRC-unsafe EFP observables are shown in Fig. 2.

A summary of all the models trained with high-level observables is shown in Table I.

III. DATASETS AND TRAINING

Samples of light quark (u, d, s) jets and gluon jets are generated in dijet events from pp collisions at $\sqrt{s}$=14 TeV. Collisions and immediate decays are generated with MADGRAPH5 v2.6.5 [28], while showering and hadronization is simulated with PYTHIA v8.235 [29]. The light quark-initiated jets come from the parton level hard-processes $pp \to qq$ and $q\bar{q}$ while the gluon-initiated jets come from $pp \to gg$. Mixed quark and gluon states are not generated to minimize ambiguity, as precise theoretical definitions of quark/gluon jet labels are generally elusive [9], though operational jet flavor definitions [30, 31] may be used to classify quark and gluon jets directly in LHC data. To compare the effects of particle hadronization on quark/gluon jet tagging, the events are generated with and without hadronization effects, respectively corresponding to "hadron" and "parton" level events, by toggling the HADRONLEVEL:ALL switch in PYTHIA. Jets are then passed through the DELPHES v3.4.2 [32] detector simulator, using the standard ATLAS card, to simulate interactions with the detector[3]. No additional pp interactions (pileup) are considered, as many studies have shown effective mitigation techniques to attenuate the effects of pileup [33–35].

Jets are reconstructed from calorimeter towers with the anti-k_T clustering algorithm [36], as implemented in FASTJET v3.3.2 [37], with a distance parameter of $R = 0.4$ and disregarding neutrinos. In each event, only the hardest jet with absolute pseudorapidity $|\eta| < 2.0$ is kept.

To study energy dependence, three ranges of jet p_T are considered: $200 - 220$ GeV, $500 - 550$ GeV, and $1000 - 1100$ GeV, with the threshold applied to reconstructed jets. For efficiency of generation, similar thresholds are applied at parton-level, but with a window 20% broader to avoid distortions.

For each jet p_T range, 650k quark jets and 650k gluon jets are generated; these are split into datasets with 1M events for training, 200k for testing, and 100k for validation. The sets of unordered towers used as inputs to the low-level networks – PFN, EFN, and EFN[κ] – are preprocessed by normalizing the sum of the p_T of the towers

[3] Note that detector simulations such as Delphes [32] may introduce low-p_T cutoffs, which effectively act as controlled cutoffs for IRC-unsafe observables.

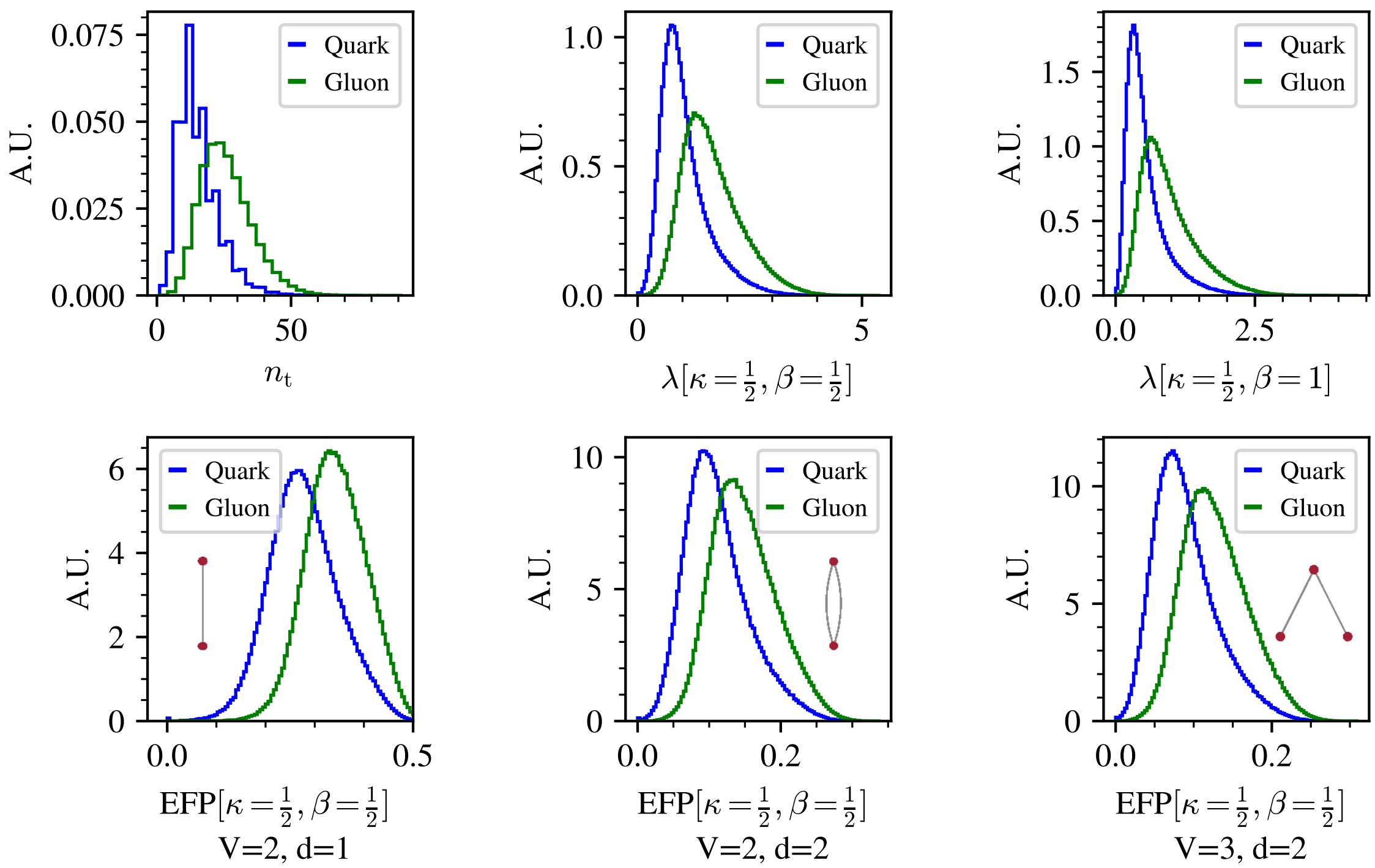

FIG. 2. Distributions of tower multiplicity and select IRC-unsafe Generalized Angularity observables (top), and IRC-unsafe EFP observables (bottom), for quark- and gluon-initiated jets with $p_T \in [500, 550]$ GeV. The shape of the EFP multigraphs is shown for illustrative purposes.

TABLE I. Summary of the models trained on IRC-safe and IRC-unsafe jet observables.

Model Name	Description	Number of Observables
DNN[safe]	DNN trained on N-subjettiness variables and jet mass.	19
DNN[safe, n_t, $\lambda[\frac{1}{2}, \beta]$]	DNN trained on N-subjettiness variables, jet mass, tower multiplicity, and a generalized angularity variable with $\kappa = \frac{1}{2}$ and $\beta \in \{\frac{1}{2}, 1, 2\}$.	21
LDA[safe]	LDA trained on IRC-safe EFP variables ($d \leq 5$) with $\beta = \frac{1}{2}$.	102
LDA[safe, n_t, EFP$[\frac{1}{2}, \beta]$]	LDA trained on IRC-safe EFP variables ($d \leq 5$) with $\beta = \frac{1}{2}$, tower multiplcity, and IRC-unsafe EFP variables ($d \leq 5$) with $\kappa = \frac{1}{2}$ and $\beta \in \{\frac{1}{2}, 1, 2\}$.	205

in the sets to unity. The observables used as inputs to the high-level classifiers – DNN and LDA – are preprocessed by subtracting the mean and dividing by the standard deviation of the distributions in the training set. See the Appendix for details on network architectures and training. The performance of the various classification strategies is compared using the area under the receiver operating curve (AUC) of each network. The statistical uncertainty on the strategies is measured using boostrapping to $\pm$ 0.002 or less, unless otherwise specified.

IV. RESULTS AND DISCUSSION

The PFNs, which provide a loose upper limit, perform well, with classification power increasing with jet p_T as shown in Tab. II. The EFNs, which are limited to IRC-safe information, show a small but statistically significant drop in relative performance. The difference in the EFNs and PFNs internal constraints allows us to conclude that the difference in performance is due to the use of IRC-unsafe information by the PFNs, which grows modestly in importance with jet p_T.

To understand the physical source of the IRC-unsafe information, we train EFN and PFN networks on events at parton and hadron level. In the parton level events, the PFN-EFN gap vanishes (see Tab. III), confirming the results of Ref. [38] and demonstrating the central conclusions of Ref. [13]; without hadronization effects only IRC-safe information is needed for quark-gluon tagging. In addition, this comparison reveals that the IRC-unsafe information is introduced in the non-perturbative hadronization process. The contrast in quark and gluon jets simulated with and without hadronization effects can

TABLE II. Comparison of the quark-gluon classification performance of EFN and PFN networks, via AUC, on jets with hadronization effects included.

Jet p_{T} Range	EFN	PFN	Δ(PFN-EFN)
200-220 GeV	0.814 ± 0.001	0.828 ± 0.001	0.014 ± 0.002
500-550 GeV	0.819 ± 0.001	0.838 ± 0.001	0.019 ± 0.002
1000-1100 GeV	0.827 ± 0.001	0.848 ± 0.001	0.021 ± 0.002

TABLE III. Comparison of the quark-gluon classification performance of EFN and PFN networks, via AUC, on jets with no hadronization effects included.

Jet p_{T} Range	EFN	PFN	Δ(PFN-EFN)
200-220 GeV	0.739 ± 0.001	0.737 ± 0.001	-0.002 ± 0.002
500-550 GeV	0.753 ± 0.001	0.750 ± 0.001	-0.003 ± 0.002
1000-1100 GeV	0.759 ± 0.001	0.758 ± 0.001	-0.001 ± 0.002

be seen in observables sensitive to the number of non-perturbative emissions, such as tower multiplicity, as illustrated in Fig. 3. The number of towers in quark and gluon jets increases when including hadronization effects, indicating that despite low-p_{T} detector cutoffs, calorimeter towers may be sensitive to non-perturbative emissions, resulting in statistically significant contributions to quark/gluon jet classifiers.

PFNs are very flexible networks, allowing a vast space of possible functions. To understand how the PFNs capture the IRC-unsafe information, we seek to narrow the scope of possible functional forms. First, we attempt to narrow down the energy weighting exponents of the necessary IRC-unsafe information by comparing the performance of EFN[κ]s for the range of values $\kappa \in \{-1, -\frac{1}{2}, -\frac{1}{4}, \frac{1}{4}, \frac{1}{2}, \frac{3}{2}\}$. The selected range covers both softer and harder radiation, as large values of κ accentuate harder hadrons while small values of κ accentuate softer hadrons.

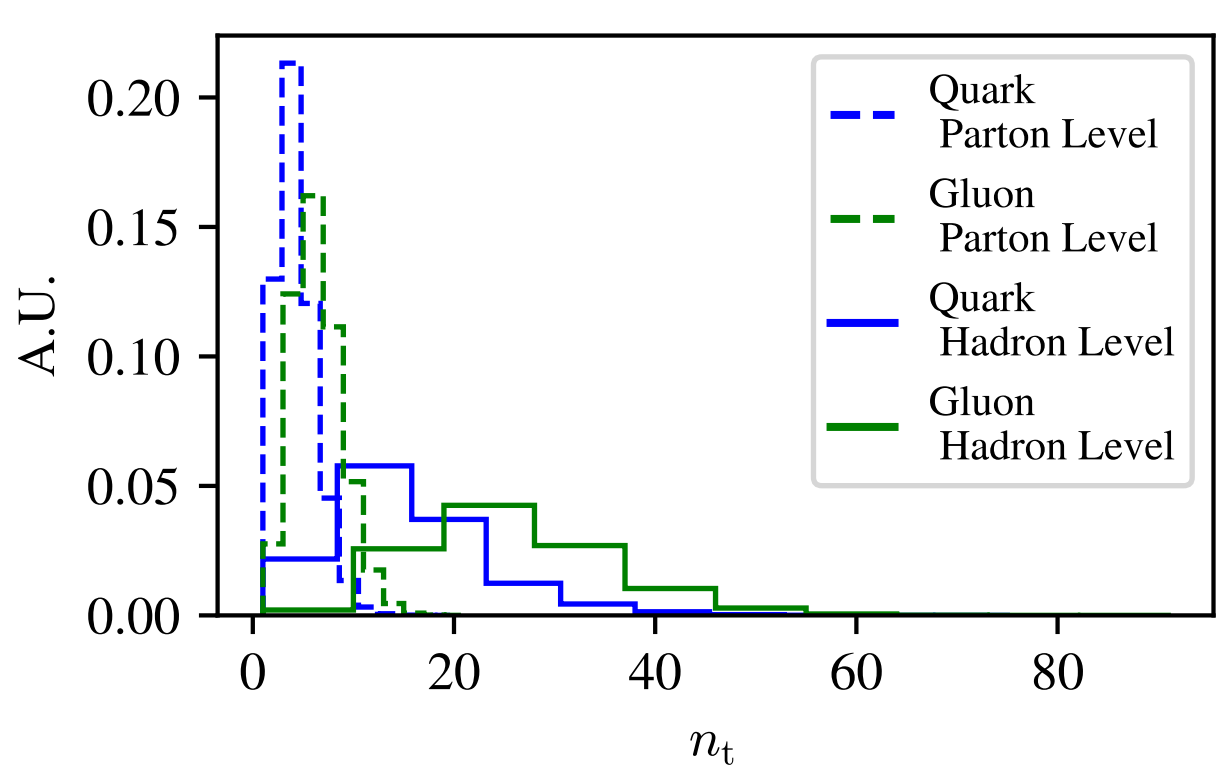

FIG. 3. Distributions of tower multiplicity (n_{t}) for quark- and gluon-initiated jets with $p_{\mathrm{T}} \in [500, 550]$ GeV, simulated with hadronization effects (solid line) and without hadronization effects (dashed line).

As shown in Tab. IV and Fig. 4, EFN[κ] performs well for energy weighting exponents close to zero, with the best performing values between $\frac{1}{4} \leq \kappa \leq \frac{1}{2}$. This indicates that the IRC-unsafe information in the PFN-EFN gap is mainly due to soft radiation, and can potentially be captured by observables with small energy weighting exponents. In addition, we note how soft radiation becomes more relevant with higher jet p_{T}, as the EFN[$\kappa = \frac{1}{4}$] and the EFN[$\kappa = \frac{1}{2}$] increasingly outperform the EFN as energy increases. For simplicity, we take $\kappa = \frac{1}{2}$ to be the critical energy weighting exponent as it consistently outperforms or effectively matches the other κ values.

Having isolated the critical energy weighting exponent which captures the IRC-unsafe information, the next step is to identify the critical angular weighting exponent, β. However, unlike the energy weighting, the EFN structure does not allow us to easily constrain the critical angular weighting values. Instead, we search for a set of observables with specific angular weighting exponents which can be combined with IRC-safe observables to approximate the PFN performance. We consider IRC-unsafe observables with energy weighting exponent $\kappa = \frac{1}{2}$ and angular weighting exponent $\beta \in \{\frac{1}{2}, 1, 2\}$, to cover narrow- and wide-angle radiation. A summary of the high-level models and the corresponding IRC-safe and IRC-unsafe observables used in the search is shown in Table I.

The results for the traditional features (N-subjettiness, jet mass, tower multiplicity, and IRC-unsafe generalized angularities) are shown in Table V and illustrated in Figure 5. These traditional observables fail to capture sufficient IRC-safe and IRC-unsafe information to match the PFN in all energy ranges.

The results for the LDA models using EFPs and tower multiplicity are shown in Table VI and illustrated in Figure 6. In contrast to the traditional features, IRC-safe EFPs largely capture the IRC-safe information used by the EFNs; in addition, there is a boost in performance when combining them with IRC-unsafe EFPs with small angular weighting exponents such as $\beta = \frac{1}{2}$, nearly matching the PFN performances[4]. The boost in performance provided by the IRC-unsafe observables increases with energy range, which is consistent with the results illustrated in Fig. 4, corroborating the importance of IRC-unsafe observables for jets with higher p_{T}. Although less compact than the traditional observables, EFPs are more effective at capturing the necessary information for quark/gluon classification.

[4] LDA models trained on IRC-safe and IRC-unsafe EFPs with $d <= 6$ and $d <= 7$ are also considered, in each case providing a marginal improvement in AUC, at the cost of significantly more EFP variables. LDA models with EFPs with $d <= 5$ are thus chosen in this paper as they result in a good approximation of the PFN performances while having a manageable size of EFP variables.

TABLE IV. Comparison of the quark-gluon classification performance of EFN[κ], classified by p_T range and $\kappa \in \{-1, -\frac{1}{2}, -\frac{1}{4}, \frac{1}{4}, \frac{1}{2}, \frac{3}{2}\}$. See Fig. 4 for a visual representation and comparison to EFP and PFN performance.

Jet p_T range	EFN[$\kappa = -1$]	EFN[$\kappa = -\frac{1}{2}$]	EFN[$\kappa = -\frac{1}{4}$]	EFN[$\kappa = \frac{1}{4}$]	EFN[$\kappa = \frac{1}{2}$]	EFN[$\kappa = \frac{3}{2}$]
200-220 GeV	0.785 ± 0.001	0.788 ± 0.001	0.794 ± 0.001	0.817 ± 0.001	0.821 ± 0.001	0.815 ± 0.001
500-550 GeV	0.796 ± 0.001	0.802 ± 0.001	0.811 ± 0.001	0.830 ± 0.001	0.831 ± 0.001	0.811 ± 0.001
1000-1100 GeV	0.801 ± 0.001	0.809 ± 0.001	0.822 ± 0.002	0.842 ± 0.001	0.841 ± 0.001	0.812 ± 0.001

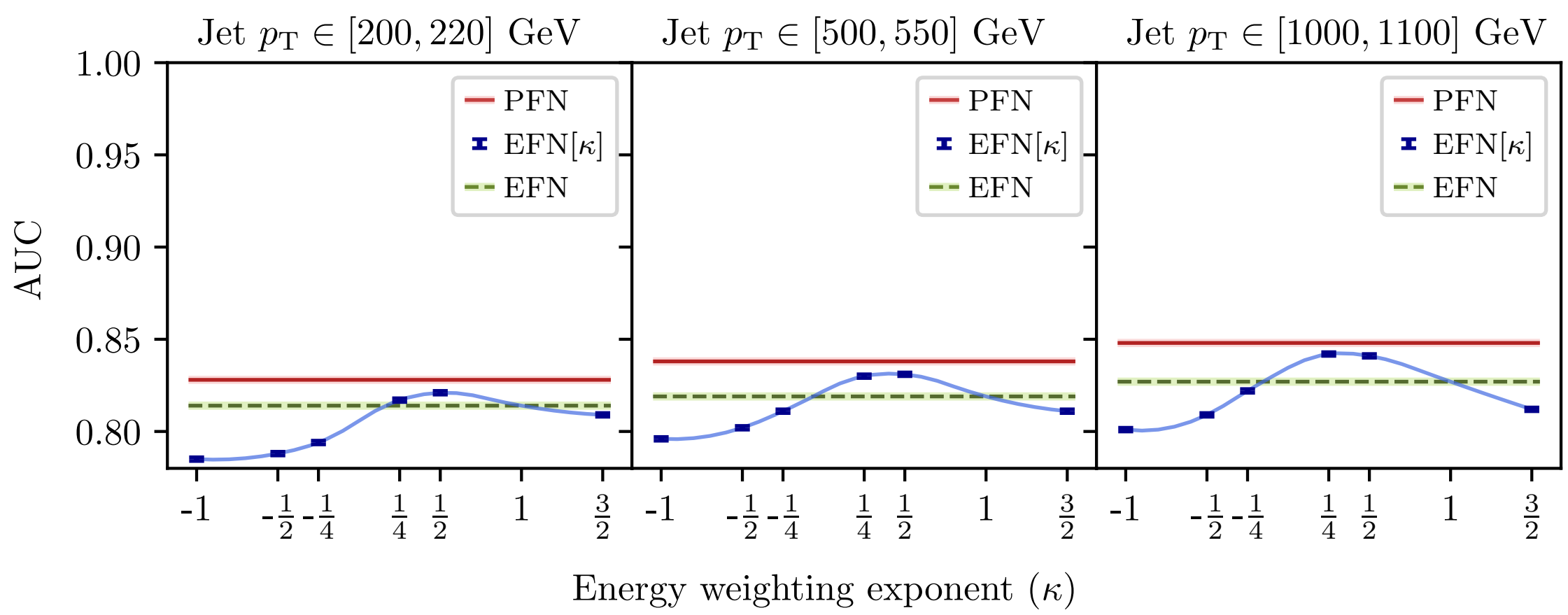

FIG. 4. Comparison of the quark-gluon classification performance, measured by AUC, of the EFN[κ]s, for several choices of the energy weighting exponent $\kappa \in \{-1, -\frac{1}{2}, -\frac{1}{4}, \frac{1}{4}, \frac{1}{2}, \frac{3}{2}\}$, which reveals the exponent necessary to exceed the performance of the IRC-safe EFN (dashed green) and approach the performance of the IRC-unsafe PFN (solid red). Solid blue lines are a quadratic interpolation of the measurements of the EFN[κ] performance at each value of κ, also given in Table IV. Three panels show the performance in the distinct jet p_T ranges.

TABLE V. AUCs of the DNN models trained on IRC-safe jet mass N-subjettiness variables, and their combinations with IRC-unsafe generalized angularities with $\kappa = \frac{1}{2}$ and $\beta \in \{\frac{1}{2}, 1, 2\}$.

Jet p_T range	DNN[safe]	DNN[safe, n_t, $\lambda[\frac{1}{2}, \frac{1}{2}]$]	DNN[safe, n_t, $\lambda[\frac{1}{2}, 1]$]	DNN[safe, n_t, $\lambda[\frac{1}{2}, 2]$]
200-220 GeV	0.804 ± 0.001	0.809 ± 0.001	0.809 ± 0.001	0.810 ± 0.001
500-550 GeV	0.815 ± 0.001	0.822 ± 0.001	0.824 ± 0.002	0.824 ± 0.001
1000-1100 GeV	0.822 ± 0.002	0.829 ± 0.002	0.831 ± 0.001	0.831 ± 0.001

TABLE VI. AUCs of the LDA models trained on IRC-safe EFPs, and their combinations with tower multiplicity and IRC-unsafe EFPs with $\kappa = \frac{1}{2}$ and $\beta \in \{\frac{1}{2}, 1, 2\}$, with $d \leq 5$ edges.

Jet p_T range	LDA[safe]	LDA[safe, n_t, EFP[$\frac{1}{2}, \frac{1}{2}$]]	LDA[safe, n_t, EFP[$\frac{1}{2}, 1$]]	LDA[safe, n_t, EFP[$\frac{1}{2}, 2$]]
200-220 GeV	0.816 ± 0.001	0.821 ± 0.001	0.820 ± 0.001	0.818 ± 0.001
500-550 GeV	0.825 ± 0.001	0.835 ± 0.001	0.834 ± 0.001	0.830 ± 0.001
1000-1100 GeV	0.826 ± 0.001	0.844 ± 0.001	0.842 ± 0.001	0.836 ± 0.001

V. CONCLUSIONS

In this work, we have confirmed that state-of-the-art machine learning models for quark/gluon jet classification are sensitive to perturbative and non-perturbative effects, the latter rooted in the hadronization process. Moreover, we have shown that the reliance of the networks on the non-perturbative IRC-unsafe information grows with jet p_T. Although the IRC-unsafe observable space is in principle infinite, its energy and angular dependence can be narrowed down by utilising the strategies introduced in this paper.

By comparing the performance of networks whose architecture constrains the models to learn functions with prescribed energy weighting forms, EFN[κ]s, we have found that most of the IRC-unsafe information can be captured by observables with small energy weighting exponents ($\frac{1}{4} \leq \kappa \leq \frac{1}{2}$). Similarly, we have performed a grid search of high-level observables with narrow cate-

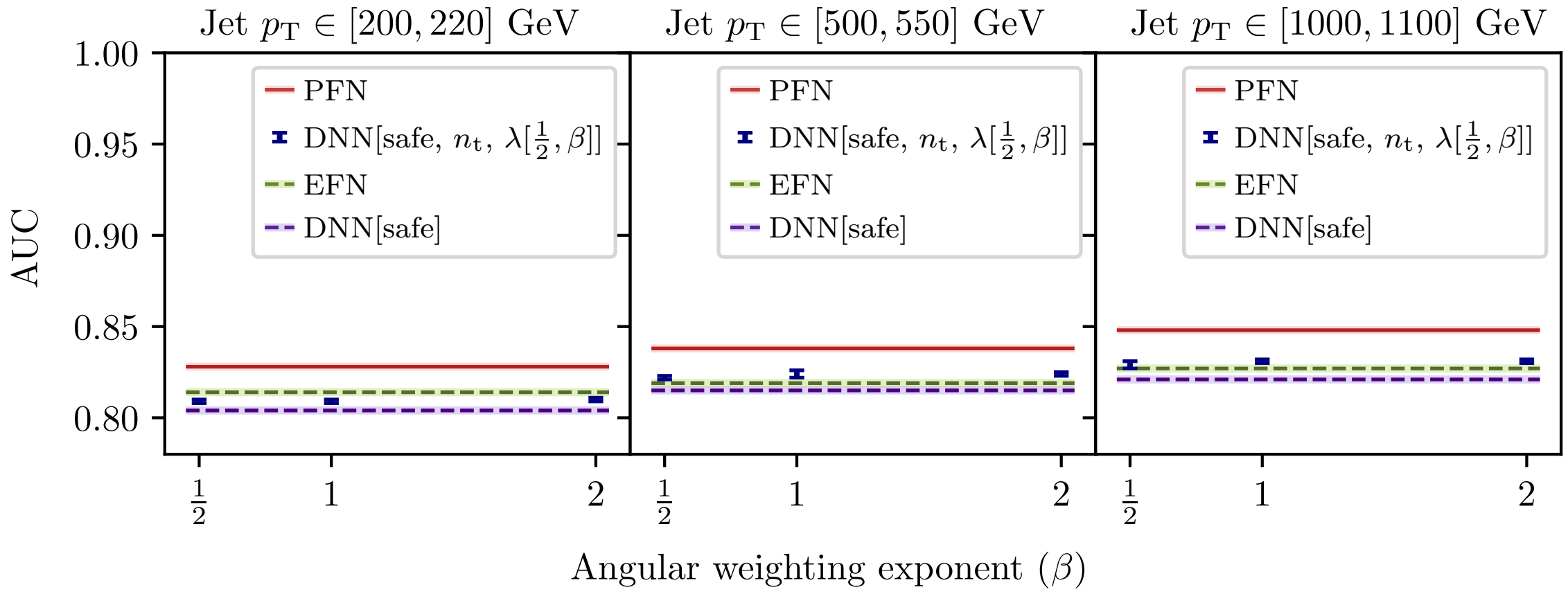

FIG. 5. AUCs of the DNN models trained on IRC-safe N-subjettiness and IRC-unsafe generalized angularity observables with $\kappa = \frac{1}{2}$ and $\beta \in \{\frac{1}{2}, 1, 2\}$, in combination with the tower multiplicity.

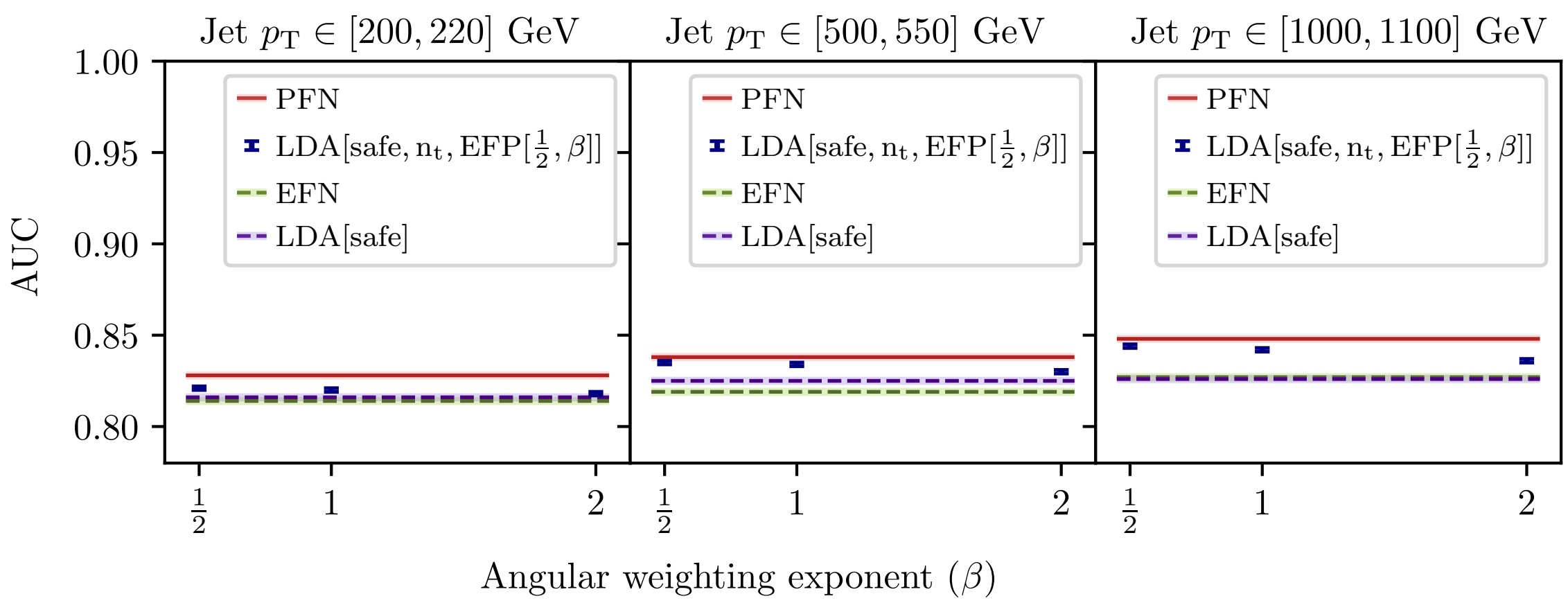

FIG. 6. AUCs of the LDA models trained on IRC-safe EFP and IRC-unsafe EFP observables with $\kappa = \frac{1}{2}$ and $\beta \in \{\frac{1}{2}, 1, 2\}$, in combination with the tower multiplicity.

gories of angular weighting factors to delimit the angular dependence of the IRC-unsafe information. The results show that most of this information can be captured by small angular weighting factors ($\beta = \frac{1}{2}$). This indicates that, as expected, IRC-unsafe information relevant for quark/gluon jet classification is due to soft, narrow-angle radiation.

Understanding the nature of the information used by deep neural networks trained for the classification of quark- vs. gluon-initiated jets, and mapping it into physics interpretable and compact jet observables, is an extremely powerful tool that could be used for analyses searching for signals beyond the Standard Model. The strategy presented in this paper allows for the interpretation of the information learned by PFNs in terms of high-level physics observables which provide a sense of the nature of the machine-learned information. This information was found to be both IRC-safe and IRC-unsafe, corresponding to perturbative and non-perturbative hadronization effects. The strategy proposed in this paper allows physicists to control and assess the systematic uncertainties of the networks by confidently including or excluding information from the learning process. In addition, this strategy can easily be extended to other analyses where having robust and interpretable observables that match the performances of deep neural networks would be a powerful tool.

ACKNOWLEDGMENTS

We wish to thank Andrew Larkoski, Ian Mount, Benjamin Nachman, Joakim Olsson, Tilman Plehn, and Jesse Thaler for their valuable feedback and insightful discussions. We also thank Wenjie Huang for his work on the initial stages on this paper. This material is based upon work supported by the National Science Foundation under grant number 1633631. DW and MF are supported

by the DOE Office of Science. The work of JC and PB in part supported by grants NSF 1839429 to PB.

Appendix A: Neural Network Hyperparameters and Architecture

Common properties across all networks include ReLu [39] activation functions for all hidden layers, and a sigmoidal output unit at the end to classify between quark and gluon jets. The low-level networks are trained using stochastic gradient descent and initialized using the He uniform weights [40]. The DNNs are trained using the Adam optimizer [41], and initialized using Glorot uniform weights [42]. In all cases, the models are optimized to minimize the relative entropy between the targets and the outputs across all training examples. All models are trained for up to 100 epochs with early stopping. The number of layers, nodes in each layer, dropout [43] rate, and the learning rate are selected using Bayesian Optimization from the Sherpa [44] optimization library. The ranges for the search of hyperparameters are shown in tables VII and VIII. All models are trained using Keras [45] from the Tensorflow package [46], with batch sizes of 128.

TABLE VII. Hyperparameter ranges for bayesian optimization of PFN, EFN, and EFN[κ] networks.

Parameter	Range
Num. of layers in the per-tower module Φ	[1, 5]
Size of the layers in the per-tower module Φ	[32, 196]
Num. of layers in the backend module F	[1, 5]
Size of the layers in the backend module F	[32, 196]
Learning rate	[0.0001, 0.01]
Learning rate decay	[0.000001, 0.001]
Dropout rate for the layers in module F	[0.0, 0.5]

TABLE VIII. Hyperparameter ranges for bayesian optimization of DNN networks.

Parameter	Range
Num. of layers	[1, 10]
Num. of units	[2, 196]
Learning rate	[0.0001, 0.01]
Dropout	[0.0, 0.5]

[1] P. Baldi, K. Bauer, C. Eng, P. Sadowski, and D. Whiteson, Jet substructure classification in high-energy physics with deep neural networks, Physical Review D **93**, 10.1103/physrevd.93.094034 (2016).

[2] D. Guest, J. Collado, P. Baldi, S.-C. Hsu, G. Urban, and D. Whiteson, Jet flavor classification in high-energy physics with deep neural networks, Physical Review D **94**, 10.1103/physrevd.94.112002 (2016).

[3] D. Guest, K. Cranmer, and D. Whiteson, Deep learning and its application to lhc physics, Annual Review of Nuclear and Particle Science **68**, 161–181 (2018).

[4] A. J. Larkoski, I. Moult, and B. Nachman, Jet substructure at the large hadron collider: A review of recent advances in theory and machine learning, Physics Reports **841**, 1–63 (2020).

[5] J. Pumplin, How to tell quark jets from gluon jets, Phys. Rev. D **44**, 2025 (1991).

[6] J. Gallicchio and M. D. Schwartz, Quark and gluon tagging at the lhc, Physical Review Letters **107**, 10.1103/physrevlett.107.172001 (2011).

[7] J. Gallicchio and M. D. Schwartz, Quark and gluon jet substructure, Journal of High Energy Physics **2013**, 10.1007/jhep04(2013)090 (2013).

[8] G. Aad, B. Abbott, J. Abdallah, S. Abdel Khalek, O. Abdinov, R. Aben, B. Abi, M. Abolins, O. S. AbouZeid, and et al., Light-quark and gluon jet discrimination in pp collisions at $\sqrt{s} = 7$TeV with the atlas detector, The European Physical Journal C **74**, 10.1140/epjc/s10052-014-3023-z (2014).

[9] P. Gras, S. Höche, D. Kar, A. Larkoski, L. Lönnblad, S. Plätzer, A. Siódmok, P. Skands, G. Soyez, and J. Thaler, Systematics of quark/gluon tagging, Journal of High Energy Physics **2017**, 10.1007/jhep07(2017)091 (2017).

[10] G. Kasieczka, N. Kiefer, T. Plehn, and J. Thompson, Quark-gluon tagging: Machine learning vs detector, SciPost Physics **6**, 10.21468/scipostphys.6.6.069 (2019).

[11] M. Andrews, J. Alison, S. An, B. Burkle, S. Gleyzer, M. Narain, M. Paulini, B. Poczos, and E. Usai, End-to-end jet classification of quarks and gluons with the cms open data, Nuclear Instruments and Methods in Physics Research Section A: Accelerators, Spectrometers, Detectors and Associated Equipment **977**, 164304 (2020).

[12] S. Choi, S. J. Lee, and M. Perelstein, Infrared safety of a neural-net top tagging algorithm, Journal of High Energy Physics **2019**, 10.1007/jhep02(2019)132 (2019).

[13] A. J. Larkoski and E. M. Metodiev, A theory of quark vs. gluon discrimination, Journal of High Energy Physics **2019**, 10.1007/jhep10(2019)014 (2019).

[14] A. J. Larkoski, J. Thaler, and W. J. Waalewijn, Gaining (mutual) information about quark/gluon discrimination, Journal of High Energy Physics **2014**, 10.1007/jhep11(2014)129 (2014).

[15] P. T. Komiske, E. M. Metodiev, and J. Thaler, Energy flow polynomials: a complete linear basis for jet substructure, Journal of High Energy Physics **2018**, 10.1007/jhep04(2018)013 (2018).

[16] T. Faucett, J. Thaler, and D. Whiteson, Mapping machine-learned physics into a human-readable space (2020), arXiv:2010.11998 [hep-ph].

[17] L. de Oliveira, M. Kagan, L. Mackey, B. Nachman, and A. Schwartzman, Jet-images — deep learning edition, Journal of High Energy Physics **2016**, 10.1007/jhep07(2016)069 (2016).

[18] P. T. Komiske, E. M. Metodiev, and M. D. Schwartz, Deep learning in color: towards automated quark/gluon jet discrimination, Journal of High Energy Physics **2017**, 10.1007/jhep01(2017)110 (2017).

[19] P. T. Komiske, E. M. Metodiev, and J. Thaler, Energy flow networks: deep sets for particle jets, Journal of High Energy Physics **2019**, 10.1007/jhep01(2019)121 (2019).

[20] H. Qu and L. Gouskos, Jet tagging via particle clouds, Physical Review D **101**, 10.1103/physrevd.101.056019 (2020).

[21] G. Louppe, K. Cho, C. Becot, and K. Cranmer, Qcd-aware recursive neural networks for jet physics, Journal of High Energy Physics **2019**, 10.1007/jhep01(2019)057 (2019).

[22] T. Cheng, Recursive neural networks in quark/gluon tagging, Computing and Software for Big Science **2**, 10.1007/s41781-018-0007-y (2018).

[23] S. Egan, W. Fedorko, A. Lister, J. Pearkes, and C. Gay, Long short-term memory (lstm) networks with jet constituents for boosted top tagging at the lhc (2017), arXiv:1711.09059 [hep-ex].

[24] A. Bogatskiy, B. Anderson, J. T. Offermann, M. Roussi, D. W. Miller, and R. Kondor, Lorentz group equivariant neural network for particle physics (2020), arXiv:2006.04780 [hep-ph].

[25] J. Thaler and K. Van Tilburg, Identifying boosted objects with n-subjettiness, Journal of High Energy Physics **2011**, 10.1007/jhep03(2011)015 (2011).

[26] J. Thaler and K. Van Tilburg, Maximizing boosted top identification by minimizing n-subjettiness, Journal of High Energy Physics **2012**, 10.1007/jhep02(2012)093 (2012).

[27] K. Datta and A. Larkoski, How much information is in a jet?, Journal of High Energy Physics **2017**, 10.1007/jhep06(2017)073 (2017).

[28] J. Alwall, R. Frederix, S. Frixione, V. Hirschi, F. Maltoni, O. Mattelaer, H.-S. Shao, T. Stelzer, P. Torrielli, and M. Zaro, The automated computation of tree-level and next-to-leading order differential cross sections, and their matching to parton shower simulations, Journal of High Energy Physics **2014**, 10.1007/jhep07(2014)079 (2014).

[29] T. Sjöstrand, S. Mrenna, and P. Skands, A brief introduction to Pythia 8.1, Computer Physics Communications **178**, 852–867 (2008).

[30] E. M. Metodiev and J. Thaler, Jet topics: Disentangling quarks and gluons at colliders, Physical Review Letters **120**, 10.1103/physrevlett.120.241602 (2018).

[31] P. T. Komiske, E. M. Metodiev, and J. Thaler, An operational definition of quark and gluon jets, Journal of High Energy Physics **2018**, 10.1007/jhep11(2018)059 (2018).

[32] J. de Favereau, C. Delaere, P. Demin, A. Giammanco, V. Lemaître, A. Mertens, and M. Selvaggi, Delphes 3: a modular framework for fast simulation of a generic collider experiment, Journal of High Energy Physics **2014**, 10.1007/jhep02(2014)057 (2014).

[33] G. Aad, B. Abbott, J. Abdallah, O. Abdinov, R. Aben, M. Abolins, O. S. AbouZeid, H. Abramowicz, H. Abreu, and et al., Performance of pile-up mitigation techniques for jets in pp collisions at $\sqrt{s} = 8$ tev using the atlas detector, The European Physical Journal C **76**, 10.1140/epjc/s10052-016-4395-z (2016).

[34] P. T. Komiske, E. M. Metodiev, B. Nachman, and M. D. Schwartz, Pileup mitigation with machine learning (pumml), Journal of High Energy Physics **2017**, 10.1007/jhep12(2017)051 (2017).

[35] J. A. Martinez, O. Cerri, M. Pierini, M. Spiropulu, and J.-R. Vlimant, Pileup mitigation at the large hadron collider with graph neural networks (2019), arXiv:1810.07988 [hep-ph].

[36] M. Cacciari, G. P. Salam, and G. Soyez, The anti-ktjet clustering algorithm, Journal of High Energy Physics **2008**, 063–063 (2008).

[37] M. Cacciari, G. P. Salam, and G. Soyez, FastJet User Manual, Eur. Phys. J. C **72**, 1896 (2012), arXiv:1111.6097 [hep-ph].

[38] S. Bieringer, A. Butter, T. Heimel, S. Höche, U. Köthe, T. Plehn, and S. T. Radev, Measuring qcd splittings with invertible networks (2021), arXiv:2012.09873 [hep-ph].

[39] V. Nair and G. Hinton, Rectified linear units improve restricted boltzmann machines vinod nair (2010) pp. 807–814.

[40] K. He, X. Zhang, S. Ren, and J. Sun, Delving deep into rectifiers: Surpassing human-level performance on imagenet classification, in *Proceedings of the IEEE International Conference on Computer Vision (ICCV)* (2015).

[41] D. P. Kingma and J. Ba, Adam: A method for stochastic optimization, CoRR **abs/1412.6980** (2014), arXiv:1412.6980.

[42] X. Glorot and Y. Bengio, Understanding the difficulty of training deep feedforward neural networks, in *Proceedings of the Thirteenth International Conference on Artificial Intelligence and Statistics*, Proceedings of Machine Learning Research, Vol. 9, edited by Y. W. Teh and M. Titterington (JMLR Workshop and Conference Proceedings, Chia Laguna Resort, Sardinia, Italy, 2010) pp. 249–256.

[43] G. E. Hinton, N. Srivastava, A. Krizhevsky, I. Sutskever, and R. Salakhutdinov, Improving neural networks by preventing co-adaptation of feature detectors, CoRR **abs/1207.0580** (2012), arXiv:1207.0580.

[44] L. Hertel, J. Collado, P. Sadowski, J. Ott, and P. Baldi, Sherpa: Robust hyperparameter optimization for machine learning, SoftwareX (2020).

[45] F. Chollet *et al.*, Keras, `https://keras.io` (2015).

[46] M. Abadi *et al.*, TensorFlow: Large-scale machine learning on heterogeneous systems (2015), software available from tensorflow.org.